Journal of Magnetic Resonance 332 (2021) 107067

Contents lists available at ScienceDirect

Journal of Magnetic Resonance

journal homepage: www.elsevier.com/locate/jmr

Triple-pulse excitation: An efficient way for suppressing background signals and eliminating radio-frequency acoustic ringing in direct polarization NMR experiments

Fenfen Wang [a], Sanath K. Ramakrishna [b,c], Pingchuan Sun [a], Riqiang Fu [c,*]

[a] Key Laboratory of Functional Polymer Materials of the Ministry of Education and College of Chemistry, State Key Laboratory of Medicinal Chemical Biology, Nankai University and Collaborative Innovation Center of Chemical Science and Engineering, Tianjin 300071, China
[b] Department of Chemistry and Biochemistry, Florida State University, Tallahassee, FL 32306, USA
[c] National High Magnetic Field Laboratory, Florida State University, 1800 East Paul Dirac Drive, Tallahassee, FL 32310, USA

ARTICLE INFO

Article history:
Received 19 July 2021
Revised 6 September 2021
Accepted 11 September 2021
Available online 14 September 2021

Keyword:
Direct polarization
Single-pulse excitation
Triple-pulse excitation
Acoustic ringing
Background suppression

ABSTRACT

Direct polarization using a single pulse is the simplest excitation scheme in nuclear magnetic resonance (NMR) experiments, capable of quantifying various compositions in many materials applications. However, this single-pulse excitation generally gives rise to NMR spectra with a severely distorted baseline due to the background signals arising from probe components and/or due to the radio-frequency (RF) acoustic ringing, especially in low-γ nuclei and wide-line NMR. In this work, a triple-pulse excitation scheme is proposed to simultaneously suppress the background signals and eliminate the RF acoustic ringing. The acoustic ringing is cancelled through subtraction in any two consecutive scans by alternating the receiver phase while keeping the phase of the pulse right before acquisition the same. While the triple-pulse scheme generates an additional flip-angle dependent scaling to the traditional single-pulse excitation profile in such a way that the scaling is one when the flip-angle is $\sim$90° but becomes almost zero when the flip-angle is very small. Therefore, the background signals arising from the materials outside the sample coil experiencing a very small fraction of the RF flip-angles can be effectively suppressed. Various samples containing ^{1}H and quadrupolar nuclei (^{17}O, ^{25}Mg, and ^{23}Na) have been used to demonstrate the effectiveness of this newly proposed triple-pulse excitation in terms of suppressing the background signals and eliminating the acoustic ringing effects.

1. Introduction

Nowadays, direct polarization using a single-pulse excitation scheme remains to be a frequently used method in many nuclear magnetic resonance (NMR) applications such as catalysts/zeolites, batteries, silicates, polymer, etc. [1–12], where either no abundant spin is available in the lattice of materials to be a source for cross-polarization (CP) enhancement or the CP efficient is rather low, while a rapid direct polarization is possible for those nuclei having a very short spin–lattice relaxation time (T_1). As shown in Fig. 1a, the single-pulse (SIP) excitation represents the simplest direct polarization scheme in NMR by flipping the magnetization away from its equilibrium state in the longitudinal direction (+z axis). The projection of the tilted magnetization onto the horizontal plane (the xy plane) generates transverse magnetization that is detected by the receiver. However, the SIP excitation polarizes all signals within the range of the magnetic field generated by the radio-frequency (RF) pulse, including possible background signals from probe materials (such as capacitors, stator, etc.) located outside the sample coil. In addition, the deadtime ringdown effects, which arise from the acoustic ringing of the RF pulse right before the receiver opening, often cause a wiggling or distorted baseline in the observed spectra [13,14], particularly in low-γ nuclei (such as ^{17}O and ^{25}Mg) and wide-line NMR. Typically, the background signals and the distorted baseline intrinsically exist in the SIP-excited spectra.

Many approaches [13–23] have been proposed to suppress the background signals and acoustic ringing. In principle, both backgrounds and acoustic ringing effects can be simultaneously removed by subtracting two separate experiments with and without the sample in the probe under identical conditions. However, such a standard procedure is not practical for two reasons. (1) The total experimental time is doubled. One of the experiments

* Corresponding author at: National High Magnetic Field Lab, 1800 East Paul Dirac Drive, Tallahassee, FL 32310, USA.
E-mail address: rfu@magnet.fsu.edu (R. Fu).

https://doi.org/10.1016/j.jmr.2021.107067
1090-7807/

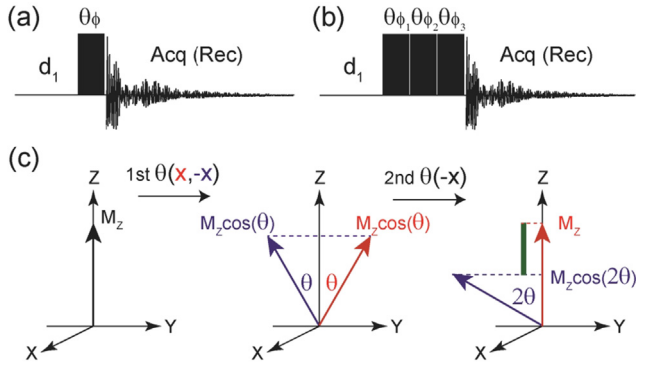

Fig.1. Pulse sequences used for direct polarization NMR experiments. (a) A single-pulse excitation, where ϕ is (x, −x, y, −y) and the corresponding phase for the receiver is (x, −x, y, −y). (b) A triple-pulse excitation, where the complete phase cycling is ϕ_1= (x, −x, x, −x, x, −x, x, −x, y, −y, y, −y, y, −y, y, −y), ϕ_2= (−x, −x, x, x, −x, −x, x, x, −y, −y, y, y, −y, −y, y, y), ϕ_3= (x, x, x, x, −x, −x, −x, −x, y, y, y, y, −y, −y, −y, −y) and the corresponding receiver phase is (x, −x, −x, x, −x, x, x, −x, y, −y, −y, y, y, −y, y, −y). (c) A simple vector model in the first two scans of the above phase lists for the first two pulses in (b).

does not have the sample placed in the sample coil and records only the unwanted signals and noise. As a result, the noise level in the subtracted spectrum increases by 141%. (2) The probe tuning/matching often becomes different with and without the sample being placed inside the sample coil. Change in the probe tuning/matching would alter the phase of the observed signals, so that the phase correction for the spectra recorded in the two separate experiments has to be performed independently. In light of the severely distorted baseline from the background signals and acoustic ringing effects, any slight difference in the phase correction would lead to incomplete cancellation of the background signals and acoustic ringing effects. Jaeger and Hemmann [13,14] proposed an alternative way to subtract the two spectra (called EASY, *e*limination of *a*rtifacts in NMR *s*pectroscop*y*). They ran one experiment with the sample being inside the sample coil but recorded two sets of free induction decay (FID), one after another with a short delay (much shorter than the recycle delay). The first FID, after the 90° pulse excitation, contains the wanted signals as well as all unwanted signals (including the background signals and the deadtime ringing effects). Immediately after the first FID, another 90° pulse is applied, followed by recording the second FID, such that the second FID contains only those unwanted signals since the wanted signals have completely decayed in the transverse plane. Therefore, any changes in the probe tuning/matching for acquiring these two FIDs can be avoided and the subtraction of the two FIDs (without doubling the experimental time) eliminates the background signals and acoustic ringing effects simultaneously, again at an expense of increasing the noise level by 141%.

In fact, the background signals and acoustic ringing effects are two different issues. The former are real signals of the probe materials around the sample coil induced by the applied RF pulses. Therefore, they are coherent to the phases of the RF pulses. In comparison, the acoustic ringing effects are the response of the coil to the RF pulses, which depends on the resonance frequency and probe tuning. Typically, a lower frequency exhibits a longer acoustic ringing, especially for low-γ nuclei. The acoustic ringing is not coherent to the phase of the applied RF pulses, thus it can be effectively eliminated through subtraction by alternating the receiver phase while keeping the same phase of the RF pulse prior to the receiver. CP [24] is a good example for suppressing the acoustic ringing effects, where the signals of a dilute spin are polarized during a contact time between the protons and the dilute spin when their spin-lock fields fulfill the Hartmann-Hahn matching condition [25]. In the CP experiments, the contact pulse on the dilute spin has the same phase while the receiver's phase is alternated in two consecutive scans. Due to the fact that the sign of the cross-polarized signals of the dilute spin can be altered by shifting the phase of the ^{1}H 90° pulse before the CP contact time by 180°, subtracting the two consecutive scans allows for the accumulation of the cross-polarized signals while eliminating both the acoustic ringing effects (leading to the baseline distortion) and all of the signals (including the background signals from the probe components) that are not polarized from ^{1}H through CP. A longer delay between the pulse end and the opening of the receiver (i.e., DE, the so-called deadtime) could sufficiently remove the acoustic ringing effects but may not be able to suppress the background signals, depending on the linewidth of the background signals. In addition, increasing DE induces significant phase dispersion of those signals spreading over a large spectral window before acquisition, resulting in a severe phase distortion of the wanted signals. In this regard, the spin-echo pulse sequence is the method of choice to obtain the in-phase signals over a large spectral window and at the same time to suppress the background signals as well as the acoustic ringing effects. This is because the data acquisition takes place after a relatively long refocusing delay, such that any acoustic ringing effects will be diminished completely. While the background signals are from the materials outside the sample coil and experience only a small fraction of the 180° RF flip-angle generated inside the sample coil, they cannot be refocused and will be effectively canceled out after the complete phase cycling. Bendall and Gordon [26] extensively discussed the resulting signal intensity as a function of the pulse flip-angle based on multiple spin-echo sequences, known as the DEPTH profiling, to improve spatial discrimination using surface coils that are generally encountered with notorious B_1 inhomogeneity. Since the DEPTH spectra are sensitive to the pulse flip-angle, the DEPTH sequences have been applied to suppress the background signals for spin-1/2 nuclei [17,27], but they have not been focused on eliminating acoustic ringing effects, especially in quadrupolar nuclei where the 180° RF inversion might become rather insufficient, depending on quadrupolar couplings.

Here, we design a triple-pulse (dubbed as TRIP) excitation scheme, as shown in Fig. 1b, in such a way that the phase (i.e., ϕ_3 in Fig. 1b) of the pulse right before acquisition always remains the same in any two consecutive scans while the receiver phase is alternated. Therefore, the acoustic ringing effects are cancelled through subtraction of the two consecutive signals. On the other hand, the three-pulse scheme generates an additional flip-angle dependent scaling to the SIP excitation profile in such a way that the scaling is one when the flip-angle is ~90° but it becomes significantly small when the flip-angle is less. Therefore, the background signals resulted from the probe materials outside the sample coil that experience a very small fraction of the RF flip-angles can be dramatically suppressed. In other words, without using any 180° inversion pulse as in the spin-echo based DEPTH sequences, the TRIP scheme can also achieve such a flip-angle dependent excitation profile and thus is applicable to quadrupolar nuclei. The SIP and TRIP excitation profiles will be compared using spin-1/2 systems. Various samples containing ^{1}H and quadrupolar nuclei (^{17}O, ^{25}Mg, and ^{23}Na) will be used to demonstrate the effectiveness of this TRIP excitation in terms of suppressing the background signals and eliminating the acoustic ringing effects.

2. Materials and experimental

Adamantane, sodium sulfate, magnesium hydroxide, diglycidyl ether of bisphenol A (DER332) and $H_2^{17}O$ (74% ^{17}O) were purchased from Sigma-Aldrich. Glutaric anhydride and zinc acetate were pur-

chased from Aladdin. All other reagents and solvents were used as received without further purification.

^{17}O enriched glutaric acid (GA-^{17}O) was first obtained by hydrolysis of glutaric anhydride. Glutaric anhydride (3.423 g, 0.03 mol) and $H_2^{17}O$ (0.76 g, 0.04 mol) were added into a 50 mL round-bottom flask with 10 mL acetone. The mixture was refluxed for 3 h. The solvent was removed by rotary evaporation to obtain a white powder solid. Then, the vitrimer network sample (labeled as TDDER) was then synthesized from DER332 (3.4 g, 0.01 mol) and GA-^{17}O (1.83 g, 0.01 mol) dissolved in DMF. The zinc acetylacetonate (5% of epoxy equivalent) as catalyst was added into the mixture, then sonicated and heated to disperse or completely dissolve. The homogenized mixture was transferred to a PTFE module, kept in 80 °C oven for 24 h to evaporate the solvent, and cured at 140 °C for 18 h by carefully increasing the temperature.

^{17}O-enriched 3,3′-phenoxy-dipropyl glutarate (labeled as ^{17}O-PDG) was synthesized for liquid-state ^{17}O NMR experiment. 2.15 g 3-bromo-1-phenoxypropane, 0.396 g ^{17}O-glutaric acid, 0.828 g K_2CO_3, 0.1 g tetrabutylammonium bromide (TBAB), and 5 mL CH_3CN were mixed together and refluxed under 110 °C for 44 h. After evaporation of the solvent, the crude product was purified by column chromatography (hexane: ethyl acetate = 50:1 to 20:1 v/v).

The metal organic framework $[(CH_3)_2NH_2]Mg(HCOO)_3$ (labeled as Mg-MOF) sample was prepared using the method similar to the one described in the literature [28] with some minor modifications [29]. A 23 mL solution of 50 vol% dimethylformamide (DMF) in nanopure water into which 85.0 mM $MgCl_2$ and 2 μM $MnCl_2$ (0.002%) were dissolved was sealed in a 35 mL pressure vessel. The pressure vessel was then heated to 140 °C for two days, then allowed to cool to room temperature. Once cool, the supernatant was decanted. Single crystals were obtained by slowly evaporating the solution in a 10-dram glass vial with a 1-inch diameter.

The adamantane sample was packed into a 4-mm Bruker MAS rotor and used for ^1H NMR experiments, while the sodium sulfate and sodium chloride were physically mixed (at 20:1 ratio by weight) and packed into a 4-mm Bruker MAS rotor for ^{23}Na NMR experiments. Both ^1H and ^{23}Na NMR measurements were performed on a Bruker Avance 600 MHz NMR spectrometer operating at the ^1H and ^{23}Na Larmor frequencies of 600.13 and 158.75 MHz, respectively. The sample spinning rate was controlled by a Bruker pneumatic MAS unit at 12 kHz ± 3 Hz. The ^1H 180° pulse length was calibrated to be 8.25 μs. 16 scans were used to accumulate the signals with a recycle delay of 5 s. The ^{23}Na 180° pulse length was calibrated to be 7.25 μs by monitoring the signal of NaCl that possesses null electric field gradient due to the symmetric structural arrangement in the lattice. The NaCl signal was used for chemical shift reference at 0 ppm. 2 scans were used for the SIP excitation and 4 scans for the TRIP excitation, with a recycle delay of 150 s.

The TDDER vitrimer sample was packed into a 3.2 mm pencil MAS rotor for ^{17}O NMR measurements on an 800 MHz NMR spectrometer equipped with a Bruker NEO console where the ^{17}O Larmor frequency is 108.44 MHz. The sample spinning rate was controlled by a Bruker pneumatic MAS III unit at 16 kHz ± 3 Hz. The ^{17}O 90° pulse length was calibrated to be 3.0 μs using natural abundance water, which was also used as a reference at 0 ppm. For the measurements on the TDDER sample, 1.0 and 2.0 μs were used as 90° and 180° pulse length. For the rotor-synchronized Hahn-echo and TRIP experiments, 102,400 scans were used to accumulate the signals, while 10,240 scans were used for the SIP excitation, with a recycle delay of 0.4 s. A total of two-rotor period (i.e., 125 μs) was used in the rotor-synchronized Hahn-echo experiment. The deadtime between the end of the RF pulse and the beginning of the receiver opening was set to 5 μs in the SIP and TRIP experiments.

The Mg-MOF sample was packed into a 3.2 mm pencil rotor for ^{25}Mg NMR measurements on an 800 MHz NMR spectrometer equipped with a Bruker NEO console where the ^{25}Mg Larmor frequency is 48.95 MHz. The sample spinning rate was controlled by a Bruker pneumatic MAS III unit at 16 kHz ± 3 Hz. The ^{25}Mg 90° pulse length was calibrated to be 6 μs using $MgCl_2{\cdot}6H_2O$ powder, purchased from Fisher Scientific. Different from the anhydrous $MgCl_2$ that exhibits a large ^{25}Mg quadrupolar coupling [30], this hydrous form does not show any second-order quadrupolar line-broadening (c.f. Fig. S1 in the Supporting Information) and thus is used as a ^{25}Mg reference at 0 ppm. 102,400 scans were used for signal averaging in both SIP and TRIP excitation schemes with a recycle delay of 1 s.

The liquid-state ^{17}O NMR experiments were performed on a Bruker Avance III 400 MHz NMR spectrometer with ^{17}O Larmor frequency of 54.24 MHz. The ^{17}O 90° pulse length was calibrated to be 40 μs, and DE was set to 10 μs. 3000 scans were used for both SIP and TRIP excitation schemes to accumulate the signal of ^{17}O-PDG with a recycle delay of 0.4 s.

3. Results and discussion

It is well known that, for spin-1/2, with the assumption that the B_1 field generated by the RF pulse is much stronger than any internal spin interaction, the projected signal intensity in the xy plane in the SIP excitation (Fig. 1a) follows a sine wave with respect to the pulse length τ_p:

$$S_{obs} = sin(2\pi\nu_1\tau_p) \quad (1)$$

The RF flip-angle is defined as $\theta = \nu_1\tau_p$, where ν_1 is the amplitude of the RF pulse. Therefore, for spin-1/2, ν_1 represents the nutation frequency of the polarized signal under the RF pulse. Fig. 2a shows the ^1H spectra of adamantane at different τ_p using the SIP excitation as in Fig. 1a. Clearly, in addition to the adamantane peaks (the centerband appearing at 1.63 ppm and its first sidebands at 21.8 and −18.5 ppm), there exists a very broad signal along the baseline (the enlarged baseline is shown in the inset). While the adamantane ^1H signals reach the maximum when τ_p = 4.25 μs (i.e., θ = 90°) as described by Eq. (1), the broad signal gains its intensity as τ_p increases. In other words, the broad signal arises from materials outside the sample coil. Although those

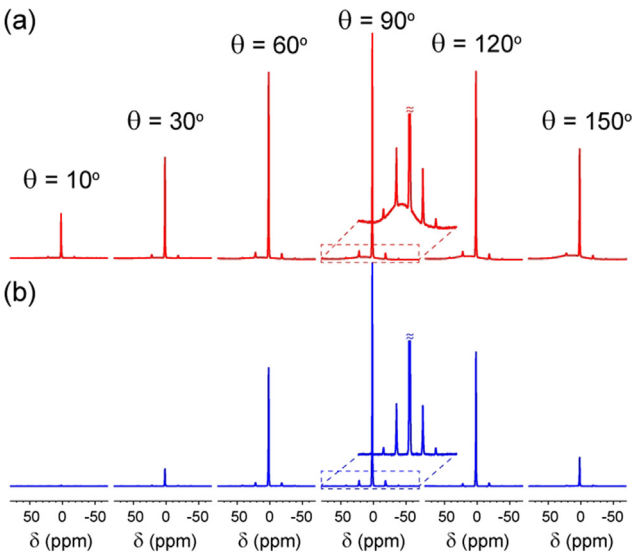

Fig.2. ^1H spectra of adamantane from a 4-mm Bruker MAS probe at different τ_p using (a) single-pulse and (b) triple-pulse excitation schemes.

materials experience a much weaker RF field than the adamantane sample inside the sample coil, their ^{1}H signal should still be polarized by the RF pulse generated inside the sample coil, resulting in the so-called background signals.

Fig. 1b shows the TRIP excitation scheme, where three pulses having different phases are applied one after another. A minimal of four scans is required to ensure the cancellation of the acoustic ringing effects by alternating the receiver phase while keeping the phase ϕ_3 of the 3rd RF pulse unchanged. Fig. 2b shows the ^{1}H spectra of adamantane at different τ_p using the TRIP excitation. Different from Fig. 2a, the adamantane ^{1}H resonances are almost invisible when $\tau_p = 0.5$ μs ($\theta \sim 10°$) but become as intense as in Fig. 2a when $\tau_p = 4.25$ μs ($\theta = 90°$), while the broad signal observed in Fig. 2a is no longer visible in all spectra (the enlarged baseline is shown in the inset). In other words, the background signal is effectively suppressed with the TRIP scheme. As indicated in Fig. 2 and in the superimposed spectra (c.f. Fig.S2 in Supporting Information), there is no difference in the signal-to-noise ratio between the TRIP and SIP schemes when $\theta = 90°$.

Fig. 1c shows the simple vector model in the first two scans of the phase cycling for the first two pulses in the TRIP scheme, the red magnetization representing the vector motion for the first scan, while the purple one for the second scan. Clearly, after the two pulses the magnetization along the z-axis remains fully in the first scan, but is scaled by cos(2θ) in the second scan. Any magnetization remaining in the xy plane will be canceled in the third and fourth scans. Thus, a minimal of four scans is required to make sure that only the magnetization along the z-axis is effectively prepared before the third pulse. As in the standard SIP scheme, the third pulse brings the magnetization along the z-axis to the xy plane for detection. It is obvious that, in every two scans, the magnetization difference along the z-axis (represented by the green) (because of the phase alternation for the receiver) between the first and second scans is observed. Therefore, the projected signal intensity per scan in the xy plane in the TRIP excitation can be written as:

$$S_{obs} = sin(2\pi\nu_1\tau_p)\left[1 - cos(4\pi\nu_1\tau_p)\right]/2. \quad (2)$$

Clearly, the TRIP excitation implies an additional θ-dependent scaling to the traditional SIP excitation profile (i.e., $\left[1 - cos(4\pi\nu_1\tau_p)\right]/2$). Fig. 3 shows the plots of the observed centerband ^{1}H signal of adamantane as a function of the RF flip-angle θ using the SIP and TIP excitations. It is obvious that when $\theta = 90°$, there is virtually no difference in the observed signal intensity with the SIP and TIP schemes, as verified in Fig. S2. Even at $\theta = 80°$, the observed signal intensity is 95.6% of that at $\theta = 90°$. With the recent probe technology development, the RF homogeneity across the sample region inside the sample coil has been greatly improved. An applied RF pulse generates a strong and uniform B_1 field inside the sample coil, but the same RF pulse provides a much weaker and inhomogeneous B_1 field outside the sample coil. Therefore, the sample inside the coil should experience a uniform B_1 field, such that they can be fully polarized by the SIP and TIP excitations.

When θ is small, the observed signal is significantly reduced using TRIP, as opposed to SIP. For instance, when $\theta = 20°$, 34% of the signal remains in the SIP excitation, while only 4% of the signal is polarized by the TRIP excitation, about a factor of 8 reduction. When $\theta = 10°$, 17% of the signal is polarized by the SIP excitation, but only 0.5% by the TRIP excitation, reducing by a factor of 34. Therefore, the TRIP excitation can significantly suppress the background signals from the materials outside the sample coil that experience only a small fraction of the RF flip-angle generated in the sample coil.

For low-γ nuclei such as ^{17}O, their resonance frequencies are rather low, such that there exists a notorious acoustic ringing from the RF pulses, resulting in a severely distorted baseline in their ^{17}O NMR spectra, especially at lower fields. Fig. 4 shows the ^{17}O solution NMR spectra of the ^{17}O-PDG sample using the SIP and TRIP excitation schemes. Clearly, the severely distorted baseline due to the acoustic ringing effects is observed in the SIP-excited spectrum (c.f. Fig. 4a), but completely suppressed in the TRIP-excited spectrum (c.f. Fig. 4b).

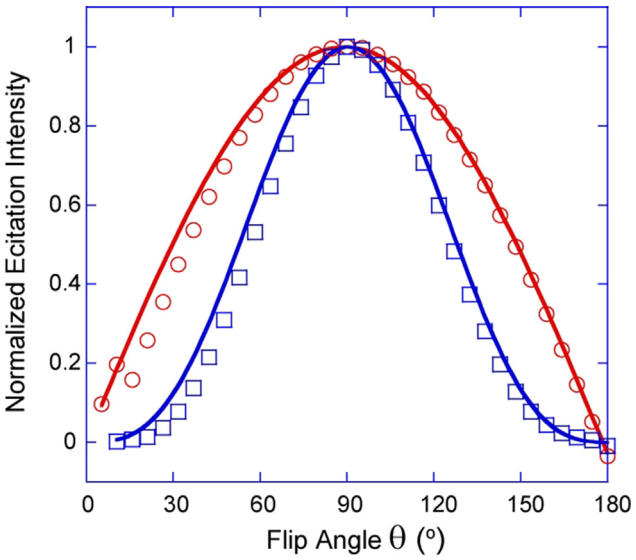

Fig.3. Profiles of the observed ^{1}H centerband signal intensity as a function of the RF flip-angle using (red open circle) single-pulse and (blue open square) triple-pulse excitation schemes. The red and blue lines are drawn respectively using Eqs. (1) and (2). (For interpretation of the references to colour in this figure legend, the reader is referred to the web version of this article.)

So far, it has been demonstrated that the TRIP excitation scheme efficiently suppresses the background signals and eliminates the acoustic ringing effects in both solid-state and solution NMR experiments. Another question to answer is whether or not it is applicable to quadrupolar nuclei in solids. For half-integer quadrupolar nuclei, the nutation under the RF pulse is highly dependent upon the ratio of ν_1/ν_q, where ν_1 and ν_q represent the RF amplitude and the quadrupolar frequency, respectively. However, the RF excitation can be simplified under these two extreme cases [31,32]: (i) $\nu_1/\nu_q \gg 0$. In this case, the RF pulse is non-selective and excites all transitions according to the nutation frequency ν_1, as described in Eq. (1); (ii) $\nu_1/\nu_q \ll 0$. In such a case,

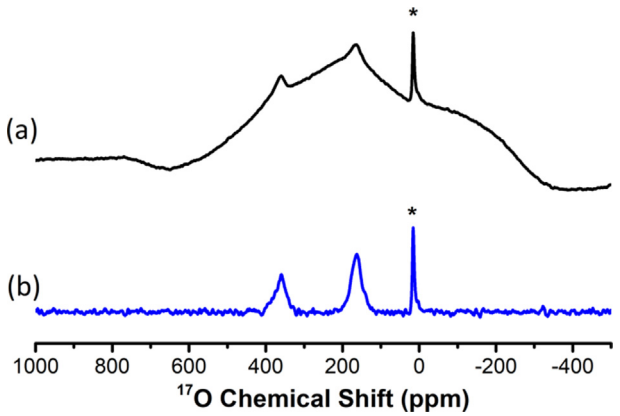

Fig.4. ^{17}O liquid-state NMR spectra of the ^{17}O-PDG using various excitation schemes at 50 °C. (a) SIP; (b) TRIP. The asterisks indicate the solvent signal from the deuterated DMSO.

the RF pulse selects only the central transition with a nutation frequency of $(I + 1/2)\ \nu_1$, where I is the spin quantum number. Therefore, for the central transition, the TRIP excitation profile can be simply modified from Eq. (2):

$$S\_obs = sin\left(2\pi\left[I+\frac{1}{2}\right]\nu_1\tau_p\right)\left\{1-cos\left(4\pi\left[I+\frac{1}{2}\right]\nu_1\tau_p\right)\right\}/2 \qquad (3)$$

Fig. 5 shows the nutation profiles of the central transitions for half-integer quadrupolar nuclei under the TRIP scheme. Clearly, due to the difference in their nutation frequencies, the signals that fulfill the condition of $\nu_1/\nu_q \gg 0$ could be easily identified by suppressing those signals from $\nu_1/\nu_q \ll 0$. For instance, for spin-3/2 nuclei, when $\nu_1\tau_p = 90°$, the maximum signals are polarized for $\nu_1/\nu_q \gg 0$ and the null signals are achieved for $\nu_1/\nu_q \ll 0$. When $\nu_1\tau_p = 45°$, the maximum signals are polarized for $\nu_1/\nu_q \ll 0$ and the signals for $\nu_1/\nu_q \ll 0$ remain at 70% using the SIP scheme (red solid-line), as opposed to 25% using the TRIP scheme (red dashed-line). As an example, Fig. 6 shows the ^{23}Na NMR spectra of the NaCl/Na_2SO_4 mixture using SIP and TRIP excitation schemes. Since NaCl does not possess the electric field gradient (EFG) due to its symmetric structural arrangement in the lattice, it belongs to the case of $\nu_1/\nu_q \gg 0$. While sodium in Na_2SO_4 exhibits a large ν_q, fulfilling the condition of $\nu_1/\nu_q \ll 0$ and thus showing a characteristic second-order quadrupolar lineshape in the spectra. It is clear that when $\tau_p = 2.0$ μs (i.e., $\nu_1\tau_p \sim 45°$), the relative NaCl signal intensity is greatly reduced when using the TRIP scheme as compared to the SIP scheme. It is worth noting that the second-order quadrupolar lineshape of the ^{23}Na MAS spectra from Na_2SO_4 is not sensitive to the pulse flip-angles (c.f., Fig. S3 in the Supporting Information). When $\tau_p = 4.0$ μs ($\nu_1\tau_p \sim 90°$), only the NaCl signal remains, while the Na_2SO_4 signal is suppressed since the ^{23}Na central transition experiences a 180° flip-angle as indicated in Fig. 6b and 6e. An interesting feature in Fig. 3 lies at θ = 180°. For the SIP excitation, there exists a single zero-crossing at θ = 180°, meaning that the inversion is extremely sensitive to the RF inhomogeneity as well as the offset effect, which can be used to precisely calibrate the pulse flip-angle. But in the TRIP profile, even at θ = 170°, the

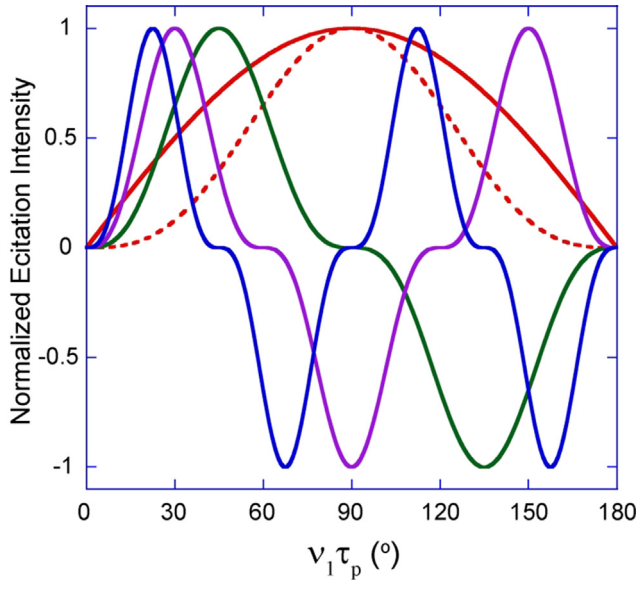

Fig.5. Nutation profiles of the central transitions for half-integer quadrupolar nuclei under the TRIP scheme. The spin-3/2, 5/2, and 7/2 nuclei are represented by green, purple, and blue lines, respectively. While the red lines refer to the nutation profiles of the signal in case of $\nu_1/\nu_q \gg 0$ under SIP (solid-line) and TRIP (dashed-line). (For interpretation of the references to colour in this figure legend, the reader is referred to the web version of this article.)

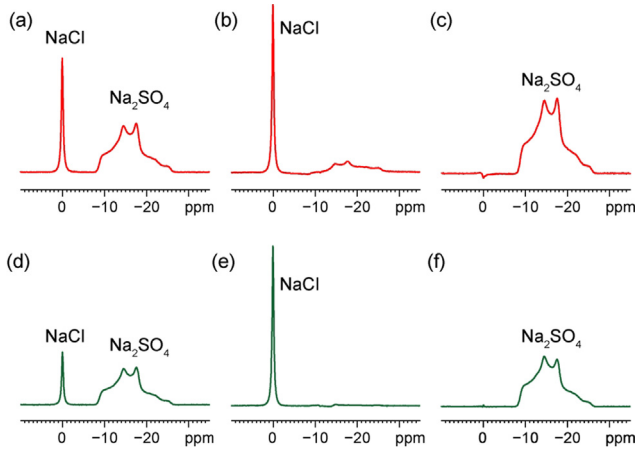

Fig.6. ^{23}Na NMR spectra of the NaCl/Na_2SO_4 mixture using SIP (red: a – c) and TRIP (green: d – f) excitation schemes. (a and d) $\tau_p = 2.0$ μs; (b and e) $\tau_p = 4.0$ μs; (c and f) difference between the spectra $\tau_p = 1.58$ and 5.75 μs. (For interpretation of the references to colour in this figure legend, the reader is referred to the web version of this article.)

observed signal is almost zero. In other words, the zero-crossing is not sensitive to the RF inhomogeneity and the offset effect. Clearly, the Na_2SO_4 signal is better suppressed in Fig. 6e than in Fig. 6b. For spectral editing purpose, the difference between the signals at $\tau_p = 1.58$ μs (i.e., $\nu_1\tau_p \sim 36°$) and $\tau_p = 5.75$ μs (i.e., $\nu_1\tau_p \sim 130°$) allows for a complete suppression of the NaCl signal. However, for $I = 5/2$, the selection of the signals for $\nu_1/\nu_q \ll 0$ could not be achieved by such a difference spectroscopy, but it may be accomplished by using the TRIP scheme. As indicated by the purple line in Fig. 5, for spin-5/2 nuclei, the signals for $\nu_1/\nu_q \ll 0$ reach their maximum polarization when $\nu_1\tau_p = 30°$. While this flip-angle polarizes only 12.5% of the signals for $\nu_1/\nu_q \gg 0$. In other words, the signals for $\nu_1/\nu_q \gg 0$ are equivalent to the background signals as they experience a small flip-angle and thus could be attenuated by using the TRIP excitation scheme, especially for higher I. Specific applications along this direction are currently underway.

Fig. 7 shows the ^{17}O NMR spectra of the TDDER vitrimer by using different excitation schemes. Vitrimers, as a new class of polymer materials with exchangeable covalent bonds as dynamic cross-links, have been envisioned to serve as fascinating functional materials with reprocessibility, self-healing ability, as well as shape memory property.[33] Since the pioneering work of vitrimers by Leibler and coworkers [34], various state-of-the-art vitrimers have been developed to explore new exchange reactions and extend their applications in various industrial fields. The topology rearrangement of vitrimers can be achieved at an elevated temperature when the associative bond exchange is activated beyond the topology freezing transition temperature, thus allowing the network to fast relax stresses and flow [33,35], leading to efficient reprocessing and recycling without loss of network integrity. As a thermally triggered associative exchange reaction, transesterification reaction has been demonstrated as a robust and convenient choice for dynamic epoxy resin vitrimers, which plays a key role in controlling the function and properties of these materials. However, such a unique dynamic behavior observed in the vitrimers is not fully understood yet, especially on a molecular level. Therefore, highly sensitive ^{17}O detection at specific sites in the exchangeable ester bond could gain deep insights into the transesterification reaction in vitrimers. ^{17}O is a low- γ nuclei with $I = 5/2$, whose ν_q is generally large and thus the extreme condition of $\nu_1/\nu_q \ll 0$ could be easily fulfilled. The acoustic ringing effects are very significant, as indicated in Fig. 7a, where the baseline is

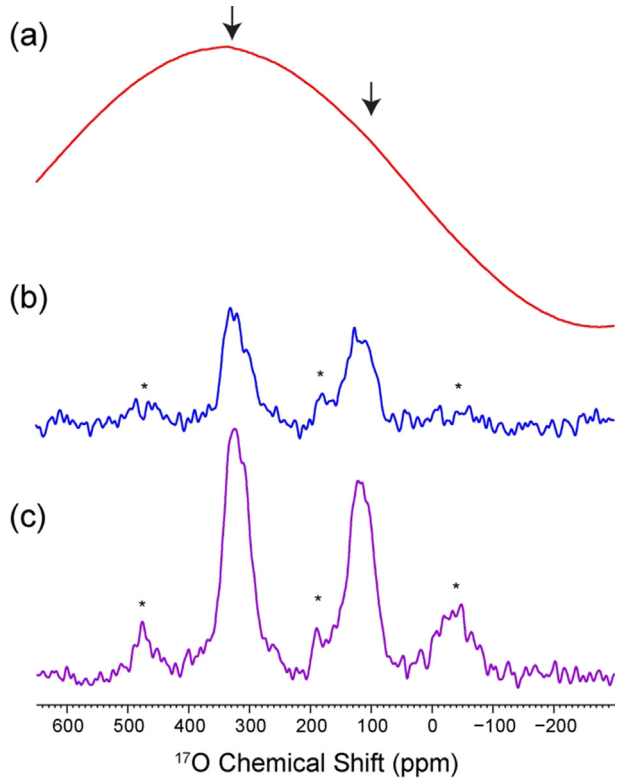

Fig.7. ^{17}O MAS NMR spectra of the TDDER vitrimer using various excitation schemes. (a) SIP; (b) rotor-synchronized Hahn-echo; (c) TRIP. The arrows indicate the positions of the ^{17}O resonances in the severely distorted baseline. The spectra shown in (b) and (c) are normalized. The asterisks indicate the spinning sidebands.

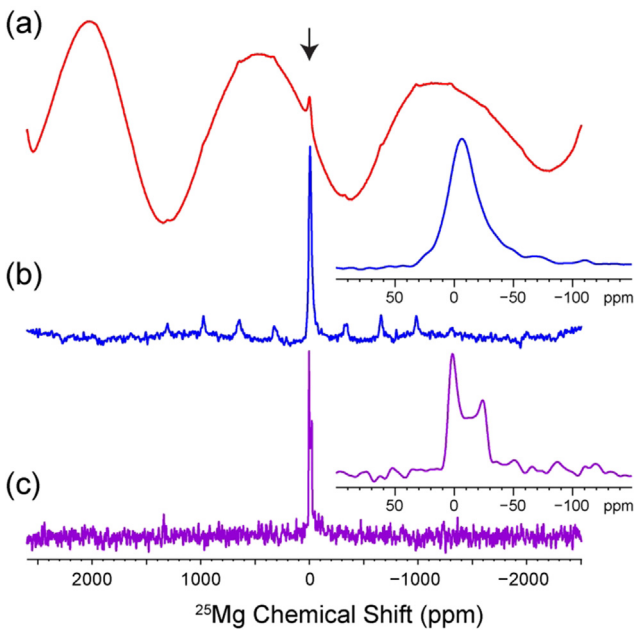

Fig.8. ^{25}Mg MAS NMR spectra recorded on the 800 MHz NMR spectrometer where the ^{25}Mg Larmor frequency is 48.95 MHz. (a) Mg-MOF using SIP; (b) Mg-MOF using TRIP; (c) $Mg(OH)_2$ using TRIP with the RAPT enhancement. The RAPT irradiation consisted of 10 pairs of Gaussian pulses (10 μs duration and ±300 kHz offset). 2048 scans were used for signal averaging with a recycle delay of 1 s.

severely distorted so that the signal at 325 ppm is barely identified while the signal at 115 ppm simply becomes invisible. With the rotor-synchronized Hahn-echo, the acoustic ringing effects are effectively eliminated such that the ^{17}O resonances at 325 and 115 ppm that are respectively assigned to the C═O and C—OH groups can be clearly observed with a good baseline (c.f. Fig. 7b). Similarly, as shown in Fig. 7c, the TRIP scheme also sufficiently suppresses the acoustic ringing effects and at the same time enhances the ^{17}O signals by a factor of two, as compared to the rotor-synchronized Hahn-echo spectrum in Fig. 7b. Although introducing a time-dependent amplitude modulation with phase-alternating unequal pulses could enhance the central transition by up to 40% [36], it does not appear to be the case for TRIP. We believe that such an enhancement (~200%) is mainly the result of without using any 180° inversion pulse in the TRIP scheme, as opposed to the spin-echo experiment that is subject to the 180° inversion efficiency in quadrupolar nuclei. [37] The signals at 325 ppm and 115 ppm should be assigned to ^{17}O for C═O and C—OH groups, respectively. Actually, two tautomers of GA-^{17}O are produced as a result of concerted double-hydrogen hopping dynamics within each dimer, leading to two ^{17}O-labelled sites in the enriched sample.[38] These two ^{17}O sites will be stabilized without tautomerism after GA-^{17}O cured into the crosslinked vitrimer network, result into two ^{17}O resonances at 325 and 115 ppm.

Another example lies in ^{25}Mg NMR. ^{25}Mg is a quadrupolar nucleus with a nuclear spin $I = 5/2$, low-gyromagnetic ratio of 2.60 MHz/T. Such a low resonance frequency often induces a long acoustic ringing, resulting in a severely distorted baseline in the NMR spectrum. Fig. 8(a and b) shows the ^{25}Mg NMR MAS spectra of the Mg-MOF sample using the different excitation schemes. This material belongs to the class of multiferroic compounds that exhibit both electric ordering (i.e., ferroelectricity) and magnetic ordering (ferromagnetism/antiferromagnetism) but its underlying ferroelectric transition mechanism has not been fully understood [29]. One of the important questions yet to be answered is the role of the Mg ionic moiety in the transition mechanism. As indicated in Fig. 8a, due to the acoustic ringing effects when using the SIP excitation scheme, the spectral baseline is severely distorted such that the lineshape of the signal as indicated by the arrow could not be revealed. The TRIP excitation scheme effectively removes the acoustic ringing effects resulting in a much better spectral baseline, as indicated in Fig. 8b. From the zoomed spectrum, the observed ^{25}Mg lineshape appears to be asymmetric. Our previous measurements [29] indicated that above the phase transition temperature (T_c = 270 K) the ^{25}Mg peak is rather broad due to the slow hopping of the organic dimethylammonium cation (DMA^+) in the MOF framework. The asymmetric ^{25}Mg lineshape observed here with the TRIP scheme may reflect such a slow motion. It is anticipated that when the temperature goes up further and the DMA^+ motion in the MOF framework is fast enough compared to the ^{25}Mg quadrupolar coupling constant, the ^{25}Mg resonance might show the characteristic second-order lineshape of the axially symmetric EFG (i.e. the asymmetric parameter $\eta_Q = 0$), similar to that shown in Fig. 8c obtained from the $Mg(OH)_2$ sample.

For quadrupolar nuclei, the sensitivity of the central transition can often be enhanced via the irradiation of the satellite transitions such as *r*otor *a*ssisted *p*opulation *t*ransfer (RAPT) [39]. In this case, the EASY schemes as proposed by Jaeger and Hemmann [13,14] require a careful adjustment of the delay between the end of the RAPT pulses and the beginning of the first 90° pulse in order to improve the suppression of the acoustic ringing effects. However, the TRIP scheme does not require additional care for suppressing the acoustic ringing. As shown in Fig. 8c, the RAPT-enhanced ^{25}Mg spectrum obtained without any delay between the end of the Gaussian pulses and the beginning of the TRIP scheme shows the excellent spectral baseline.

4. Conclusion

It has been demonstrated that a TRIP excitation scheme provides an efficient way to simultaneously suppress the background signals and eliminate the RF acoustic ringing effects. Different from the difference spectroscopy proposed in the literature [13–16], where the spectrum/FID containing only the unwanted signals (i.e., the background signals and acoustic ringing) is obtained and used to subtract it from the spectrum/FID containing both wanted and unwanted signals, the TRIP excitation generates an additional flip-angle dependent scaling to the traditional single-pulse excitation profile in such a way that the scaling is close to one when the flip-angle is close to 90° but becomes almost zero when the flip-angle is small, while the acoustic ringing is cancelled through subtraction in any two consecutive scans by alternating the receiver phase while keeping the phase of the pulse right before acquisition the same. Since the probe materials from outside the sample coil experience a very small fraction of the RF flip-angles that are generated inside the sample coil, the background signals are virtually not polarized at all and thus the wanted signals can be accumulated in every scan, rather than every other scan as in the difference spectroscopy [13–16] that increase the noise level by 141%. Such a background suppression mechanism has been utilized in the spin-echo based DEPTH sequences [17,26,27], but the TRIP scheme simultaneously suppresses the background signals and eliminates the acoustic ringing effects without using any echoes. The feature without using 180° inversion makes it applicable to quadrupolar nuclei, as opposed to the spin-echo based method where the 180° pulse required in the echo sequences could become rather insufficient for quadrupolar nuclei, thus resulting in a dramatic loss of signals. Moreover, the flip-angle dependent scaling featured in the TRIP excitation scheme could be utilized in NMR of half-integer quadrupolar nuclei to differentiate the central transitions having large quadrupolar couplings and the resonances with very small quadrupolar couplings, based on the fact that the former ones nutate $(I + 1/2)$ times faster under the RF pulses. Such a spectral editing could be very useful to simplify the spectra of quadrupolar nuclei, especially at ultra-high fields where the characteristic second-order lineshapes may become less noticeable. It is anticipated that this triple-pulse excitation scheme offers an opportunity to obtain NMR spectra free of baseline distortion in direct polarization experiments in both solid-state and liquid-state.

Declaration of Competing Interest

The authors declare that they have no known competing financial interests or personal relationships that could have appeared to influence the work reported in this paper.

Acknowledgement

All solid-state NMR experiments were carried out at the National High Magnetic Field Lab (NHMFL) supported by the NSF Cooperative agreement no. DMR-1644779 and the State of Florida.

Appendix A. Supplementary material

Supplementary data to this article can be found online at https://doi.org/10.1016/j.jmr.2021.107067.

References

[1] O.B. Lapina, Modern ssNMR for heterogeneous catalysis, Catal. Today 285 (2017) 179–193.
[2] B.E.G. Lucier, Y.N. Huang, Reviewing Ti-47/49 solid-state NMR spectroscopy: from alloys and simple compounds to catalysts and porous materials, Annu. Rep. NMR Spectros. 88 (2016) 1–78.
[3] A. Marchetti, J. Chen, Z. Pang, S. Li, D. Ling, F. Deng, X. Kong, Understanding surface and interfacial chemistry in functional nonomaterials via solid-state NMR, Adv. Mater. 29 (2017) 1605895.
[4] O. Pecher, J. Carretero-Gonzalez, K.J. Griffith, C.P. Grey, Materials' methods: NMR in battery research, Chem. Mater. 29 (2017) 213–242.
[5] A.G.M. Rankin, P.B. Webb, D.M. Dawson, J. Viger-Gravel, B.J. Walder, L. Emsley, S.E. Ashbrook, Determining the surface structure of silicated alumina catalysts via isotopic enrichment and dynamic nuclear polarization surface-enhanced NMR spectroscopy, J. Phys. Chem. C 121 (2017) 22977–22984.
[6] E. Pump, J. Viger-Gravel, E. Abou-Hamad, M.K. Samantaray, B. Hamzaoui, A. Gurinov, D.H. Anjum, D. Gajan, A. Lesage, A. Bendjeriou-Sedjerari, L. Emsley, J. M. Basset, Reactive surface organomettallic complexes observed using dynamic nuclear polarization surface enhanced NMR spectroscopy, Chem. Sci. 8 (2017) 284–290.
[7] D.A. Hirsh, A.J. Rossini, L. Emsley, R.W. Schurko, Cl-35 dynamic nuclear polarization solid-state NMR of active pharmaceutical ingredients, PCCP 18 (2016) 25893–25904.
[8] Hans Wolfgang Spiess, Interplay of structure and dynamics in macromolecular and supramolecular systems, Macromolecules 43 (13) (2010) 5479–5491.
[9] S. Dugar, N.V. Izarova, S.S. Mal, R. Fu, H.C. Joo, U. Lee, N.S. Dalal, M.T. Pope, G.B. Jameson, U. Kortz, Characterization of Pt^{IV}-containing polyoxometalates by high-resolution solid-state ^{195}Pt and ^{51}V NMR spectroscopy, New J. Chem. 40 (2016) 923–927.
[10] J. Paulino, M. Yi, I. Hung, Z. Gan, X. Wang, E.Y. Chekmenev, H.X. Zhou, T.A. Cross, Functional stability of water wire-carbonyl interactions in an ion channel, PNAS 117 (2020) 11908–11915.
[11] E.G. Keeler, V.K. Michaelis, C.B. Wilson, I. Hung, X.L. Wang, Z. Gan, R.G. Griffin, High-resolution ^{17}O NMR spectroscopy of structural water, J. Phys. Chem. B 123 (2019) 3061–3067.
[12] R. Zhang, K.H. Mroue, A. Ramamoorthy, Hydridizing cross-polarization with NOE or refocused-INEPT enhances the sensitivity of MAS NMR spectroscopy, J. Magn. Reson. 266 (2016) 59–66.
[13] C. Jaeger, F. Hemmann, EASY: a simple tool for simultaneously removing background, deadtime and acoustic ringing in quantitative NMR spectroscopy – Part 1: Basic principle and applications, Solid State Nucl. Magn. Reson. 57–58 (2014) 22–28.
[14] C. Jaeger, F. Hemmann, EASY: a simple tool for simultaneously removing background, deadtime and acoustic ringing in quantitative NMRspectroscopy. Part II: Improved ringing suppression, application to quadrupolar nuclei, cross polarisation and 2D NMR, Solid State Nucl. Magn. Reson. 63–64 (2014) 13–19.
[15] I.P. Gerothanassis, Methods of avoiding the effects of acoustic ringing in pulsed fourier transform nuclear magnetic resonance spectroscopy, Prog. Nucl. Magn. Reson. Spectrosc. 19 (1987) 267–329.
[16] I.P. Gerothanassis, Simple reference baseline subtraction - 90° pulse sequence for acoustic ringing elimination in pulsed fourier transform NMR spectroscopy, Magn. Reson. Chem. 24 (1986) 428–433.
[17] D.G. Cory, W.M. Ritchey, Suppression of signals from the probe in bloch decay spectra, J. Magn. Reson. 80 (1988) 128–132.
[18] S. Zhang, X. Wu, M. Mehring, Elimination of ringing effects in multiple-pulse sequences, Chem. Phys. Lett. 173 (1990) 481–484.
[19] J. White, L.W. Beck, D.B. Ferguson, J.F. Haw, Background suppression in MAS NMR, J. Magn. Reson. 100 (1992) 336–341.
[20] R. Fu, Z. Ma, J.P. Zheng, Proton NMR and dynamic studies of hydrous Ruthenium oxide, J. Phys. Chem. B 106 (2002) 3592–3596.
[21] Q. Chen, S.S. Hou, K. Schmidt-Rohr, A simple scheme for probehead background suppression in one-pulse ^{1}H NMR, Solid State Nucl. Magn. Reson. 26 (2004) 11–15.
[22] S. Odedra, S. Wimperis, Improved background suppression in ^{1}H MAS NMR using composite pulse, J. Magn. Reson. 221 (2012) 41–50.
[23] R. Fu, A.J. Hernandez-Maldonado, Boosting sensitivity and suppressing artifacts via multi-acquisition in direct polarization NMR experiments with small flip-angle pulses, J. Magn. Reson. 293 (2018) 34–40.
[24] A. Pines, M.G. Gibby, J.S. Waugh, Proton-enhanced NMR of dilute spins in solids, J. Chem. Phys. 59 (1973) 569–590.
[25] S.R. Hartmann, E.L. Hahn, Nuclear double resonance in rotating frame, Phys. Rev. 128 (1962) 2042–2053.
[26] M.R. Bendall, R.E. Gordon, Depth and refocusing pulses designed for multiple NMR with surface coils, J. Magn. Reson. 53 (1983) 365–385.
[27] Jian Feng, Jeffrey A. Reimer, Suppression of probe background signals via B_1 field inhomogeneity, J. Magn. Reson. 209 (2) (2011) 300–305.
[28] P. Jain, V. Ramachandran, R.J. Clark, D.Z. Hai, B.H. Toby, N.S. Dalal, H.W. Kroto, A.K. Cheetham, Multiferroic behavior associated with an order-disorder hydrogen bonding transition in metal-organic frameworks (MOFs) with the perovskite ABX3 architecture, J. Am. Chem. Soc. 131 (2009) 13625–13627.
[29] S.K. Ramakrishna, K. Kundu, J.K. Bindra, S.A. Lociero, D.R. Talham, A.P. Reyes, R. Fu, N.S. Dalal, Probing the dielectric transition and molecular dynamics in the metal–organic framework $[(CH_3)_2NH_2]Mg(HCOO)_3$ using high resolution NMR, J. Phys. Chem. C 125 (2021) 3441–3450.
[30] E.S. Blaakmeer, G. Antinucci, V. Busico, E.R.H. van Eck, A.P.M. Kentgens, Solid-state NMR investigations of $MgCl_2$ catalyst support, J. Phys. Chem. C 120 (2016) 6063–6074.

[31] A.P.M. Kentgens, J.J.M. Lemmens, F.M.M. Geurts, W.S. Veeman, Two-dimensional solid-state nutation NMR of half-integer quadrupolar nuclei, J. Magn. Reson. 71 (1987) 62–74.
[32] W.S. Veeman, Quadrupole nutation NMR in solids, Z. Naturforsch. 47a (1992) 353–360.
[33] W. Denissen, J.M. Winne, F.E. du Prez, Vitrimers: permanent organic networks with glass-like fluidity, Chem. Sci. 7 (2016) 30–38.
[34] D. Montrarnal, M. Capelot, F. Tournilhac, L. Leibler, Silica-like malleable materials from permanent organic networks, Science 334 (2011) 965–968.
[35] M. Chen, L. Zhou, Y. Wu, X. Zhao, Y. Zhang, Rapid stress relaxation and moderate temperature of malleability enabled by the synergy of disulfide metathesis and carboxylate transesterification in epoxy vitrimers, ACS Macro Lett. 8 (2019) 255–260.
[36] D. Carnevale, G. Bodenhausen, Composite pulses for efficient excitation of half-integer quadrupolar nuclei in NMR of static and spinning solid samples, Chem. Phys. Lett. 530 (2012) 120–125.
[37] A. Samoson, E. Lippmaa, 2D NMR nutation spectroscopy in solids, J. Magn. Reson. 79 (1988) 255–258.
[38] G. Wu, I. Hung, Z. Gan, V. Terskikh, X.Q. Kong, Solid-state 17O NMR study of carboxylic acid dimers: simultaneously accessing spectral properties of low- and high-energy tautomers, J. Phys. Chem. A 123 (2019) 8243–8253.
[39] H.T. Kwak, S. Prasad, T. Clark, P.J. Grandinetti, Enhancing sensitivity of quadrupolar nuclei in solid-state NMR with multiple rotor assisted population transfers, Solid State Nucl. Magn. Reson. 24 (2003) 71–77.